



# Facile preparation of superhydrophobic PDMS with patternable and controllable water adhesion characteristics

Bingpu Zhou<sup>1,\*</sup> , Yibo Gao<sup>2</sup> , Yongyun Mao<sup>1</sup> , and Weijia Wen<sup>2,3</sup> 

<sup>1</sup>Institute of Applied Physics and Materials Engineering, University of Macau, Taipa, Macau

<sup>2</sup>Environmental Science Programs, School of Science, The Hong Kong University of Science and Technology, Clear Water Bay, Kowloon, Hong Kong

<sup>3</sup>Department of Physics, The Hong Kong University of Science and Technology, Clear Water Bay, Kowloon, Hong Kong

Received: 3 May 2017

Accepted: 23 June 2017

Published online:

28 June 2017

© Springer Science+Business Media, LLC 2017

## ABSTRACT

Control of water adhesion is important for superhydrophobic surfaces in various applications. In this work, we present a facile approach to prepare superhydrophobic polydimethylsiloxane (PDMS) with patternable and controllable water adhesion capabilities. Surface grafting of N-isopropylacrylamide was primarily exploited to regulate the PDMS template morphologies, either by tuning the ultraviolet irradiation duration or adopting repeated grafting process. The surface topologies of as-prepared PDMS templates can be flexibly constructed with roughness degrees ranging widely from 1.5 to 738.7 nm. Followed with covering of carbonyl iron particles (CIP) on the template surface, the duplicated PDMS substrate can thus recur the surface topology incorporated with CIP onto the upper surface, leading to the feasibility to regulate diverse water adhesion capabilities. Owing to the synergistic effect by the surface roughness and CIP incorporation, the water adhesion capabilities of the PDMS substrates can be flexibly tuned ranging from droplet pinning to excellent water repellency. The presented strategies were further developed to create PDMS substrates with patterned water adhesion for controllable micro-droplet transportation or rapidly programmable droplet localizations. We believe that the environmentally friendly method can offer as a convenient yet cost-effective tool for future microfluidic devices, biochemical analysis, etc.

Bingpu Zhou and Yibo Gao have contributed equally to this work.

Address correspondence to E-mail: bpzhou@umac.mo

## Introduction

In nature, a variety of plants and insects exhibit inspiring non-wettable surfaces with static water contact angles (WCA) exceeding  $150^\circ$ , e.g., lotus leaf, water strider legs, and waterfowl feathers [1–4]. During the past decades, superhydrophobic surfaces have drawn rapidly increasing interests in diverse areas thanks to their attractive properties. It has now been verified that the superhydrophobic surfaces originate from the cooperative effect of surface geometry and chemical compositions [5, 6]. Inspired by natural creation, numerous methods have been successfully exploited to prepare biomimetic superhydrophobic surface [7–9]. One prevalent approach is to construct dual-scaled morphologies on surface via integrations of micro-patterning and subsequent nano-structure formation [10]. Surface fluorination is another familiar avenue to convert hydrophilic compositions for superhydrophobic surface preparation [11]. Not surprisingly, superhydrophobic surfaces/coatings have now been broadly investigated for sorts of practical applications, e.g., anti-sticking, oil/water separation, and water harvesting [12–15].

Recently, more and more attention has been focused on the manipulation of water droplets on superhydrophobic surfaces with controllable water adhesion capabilities. Superhydrophobic surfaces with water adhesion divergence have been classified into two main catalogs, namely low and high water adhesion corresponding to the Cassie–Baxter model and Wenzel model, respectively [16, 17]. Superhydrophobic surfaces with low water adhesion, termed as ‘Lotus effect,’ exhibit ultra-low adhesive force to resident water droplets, where the droplets can automatically roll off from the substrate with a small tilted angle (typically  $\sim 10^\circ$ ) [18]. On the contrary, ‘Petal effect’ was nominated to describe superhydrophobic surfaces that possess high adhesion to the water droplets, where the droplet can be pinned firmly onto the surface even when the substrate is completely turned upside down [19]. Both of ‘Lotus effect’ and ‘Petal effect’ have aroused enormous interests for practical applications. Low adhesive superhydrophobic surfaces are commonly popular for cases required of excellent water repellency, e.g., anti-fouling, self-cleaning, and drag-reduction. [20–22]. High adhesive superhydrophobic surfaces conversely are powerful for aspects demanded for no-loss droplet transfer, droplet localization, controllable reaction, biological

diagnosis, etc. [23–25]. To date, different technologies have been applied to realize the control of water adhesion on various substrates either by surface structural formation or chemical modification, e.g., ink patterning, plasma surface treatment, and laser ablation [26–28].

Polydimethylsiloxane (PDMS), one of the most frequently used materials, has attracted great attention due to the superiorities such as thermal/chemical stability, biocompatibility, and mechanical flexibility. [29, 30]. Thanks to the intrinsic low surface energy property, native PDMS surface commonly exhibits hydrophobicity with WCA around  $110^\circ$  without requirement of surface-fluorinated treatment which is typically expensive, environmentally hazardous, and toxic to human beings [31, 32]. However, the relatively high sliding angles (typically larger than  $90^\circ$ ) somehow impose restriction for applications, especially for areas emphasizing on controllable droplet transportation or programmable reaction. Researchers have recently developed various methods to prepare PDMS with controllable surface water adhesion, and the broad functionalities have been experimentally proved. For instance, Yong et al. [33] have demonstrated the utilization of femtosecond laser irradiation to fabricate micro-well arrays on PDMS films. The water adhesion exhibited extremely controllable ranges from ultra-high to ultra-low based on the overlapping of adjacent microstructures. Electrodeposition was presented to fabricate porous Ni/NiO templates with different hierarchical microstructures for PDMS replications to achieve diverse water adhesion properties [34]. The obtained PDMS substrates with high adhesive capability have been applied as ‘mechanical hands’ for lossless droplet transportation or self-cleaning surface for dust removing with low surface adhesions. Other approaches such as surface three-dimensional diffuser lithograph, curvature-induced switching, and lubricating fluid on anisotropic wrinkles have also been demonstrated to be capable of fabrication of PDMS surfaces with varying water adhesions for desired droplet ‘trap’ and ‘release’ [35–37]. However, many of the fabrication processes involve sophisticated route, expensive setup, or surface treatment, which are commonly time-consuming and harmful to the environment [38, 39]. Additionally, reports of patterned and regional water adhesion divergence on a single PDMS substrate, which could be an effective platform for application in lab-on-chip system, were

relatively limited. Instead of conventional micro-patterning and subsequent nano-engineering approach, we herein for the first time present a facile and economical method to fabricate superhydrophobic PDMS substrates with patternable and controllable water adhesion feasibility. The two-step method was composed of surface polymerization and particle inclusion. We firstly constructed the surface morphologies of PDMS templates via UV-initiated surface polymerization where the roughness extents could be simply controlled by adjusting the UV irradiation period or adopting repeated grafting approach. With subsequent CIP spreading on the template surface, the casted PDMS substrate can not only duplicate the template morphology but also include CIP onto the uppermost surface, resulting in a transition of the resident water droplet from the Wenzel state to the Cassie state. The synergistic effect from surface morphology and CIP incorporation to the adhesion properties were systematically investigated through experiments. Finally, the demonstrated strategy was developed to create patterned water adhesion variations for precise droplet motion control and localized droplet productions, etc.

## Experimental methods

### Materials

Negative photoresist (SU8-3050) was provided by MicroChem Corp. (USA) to fabricate molds on silicon wafer for construction of microfluidic chambers. Polydimethylsiloxane (PDMS) precursor and curing agent (Sylgard 184 silicone elastomer kit) were supplied by Dow Corning Corporation, USA. Carbonyl iron particles (CIP), with diameters ranging from hundreds of nanometers to several micrometers, were obtained from Sigma–Aldrich, USA, and suspended in acetone with desired concentrations for experiment. Benzophenone (Photo-initiator, 99%) and N-isopropylacrylamide (NIPAM, 97%) were purchased from Sigma–Aldrich, USA, and used for surface grafting directly without prior purification.

### Preparation of PDMS substrates with controllable surface topologies

Figure 1a depicts the structural design of the microfluidic device for liquid injection and surface

grafting. The size of the micro-chamber was defined as 18 mm × 12 mm. Briefly, negative photoresist SU8-3050 with thickness of ~500 μm was evenly spun and patterned via standard photolithography to form molds on silicon wafer. After pouring with PDMS mixture, the mold was heated at 100 °C for 2 h for PDMS solidification. The PDMS slab was then carefully peeled off from the SU8 mold with configurations of the microfluidic chamber successfully transferred. Followed with inlet/outlet punching, the PDMS replica was bonded to another PDMS substrate via 2-min oxygen plasma surface treatment. A final baking process (100 °C on hotplate for ~10 min) concluded the entire fabrication procedure for the microfluidic chip. The microfluidic device was then stored in oven (70 °C) overnight before use.

The detailed procedure to regulate surface topologies of PDMS substrates is shown in Fig. 1b. After formation of sealed micro-chamber, benzophenone (BP) was dissolved in acetone with weight ratio of ~10% and continuously infused into the micro-chamber with flow rate of 5.0 mL/h for 10 min via syringe pump (PHD 2000, Harvard Apparatus, Holliston, USA). The microfluidic device was then vacuum-dried for 10 min to remove the residual solvents. Consequently, the hydrophobic molecules (BP) can be firmly adsorbed onto the inner walls of the chamber. Degassed monomer solution (20 wt% NIPAM in deionized water) was then carefully and slowly filled into the chamber. Once fully occupied, the microfluidic platform was quickly placed onto an icepack and irradiated under ultraviolet (UV) source with fixed distance of ~10 cm between the UV lamp (~50 mW/cm<sup>2</sup>) and the microfluidic device. With the assistance of pre-absorbed BP molecules on the inner walls of the micro-chamber, NIPAM can thus be firmly grafted onto the PDMS as template with controllable surface morphologies via UV exposure. After fulfillment of preset exposure duration, the sample was removed from the curing system and the NIPAM-grafted PDMS substrate was gently detached from the microfluidic assembly, flushed with ethanol to completely remove the residuals on the substrate. In order to obtain different surface morphologies and investigate their impacts on the final wetting properties, we here have selected two different UV durations (8 and 15 min) to prepare the templates as shown in Fig. 1b. PDMS gel was then poured onto the NIPAM-grafted template, followed with degassing and solidification to replicate the surface

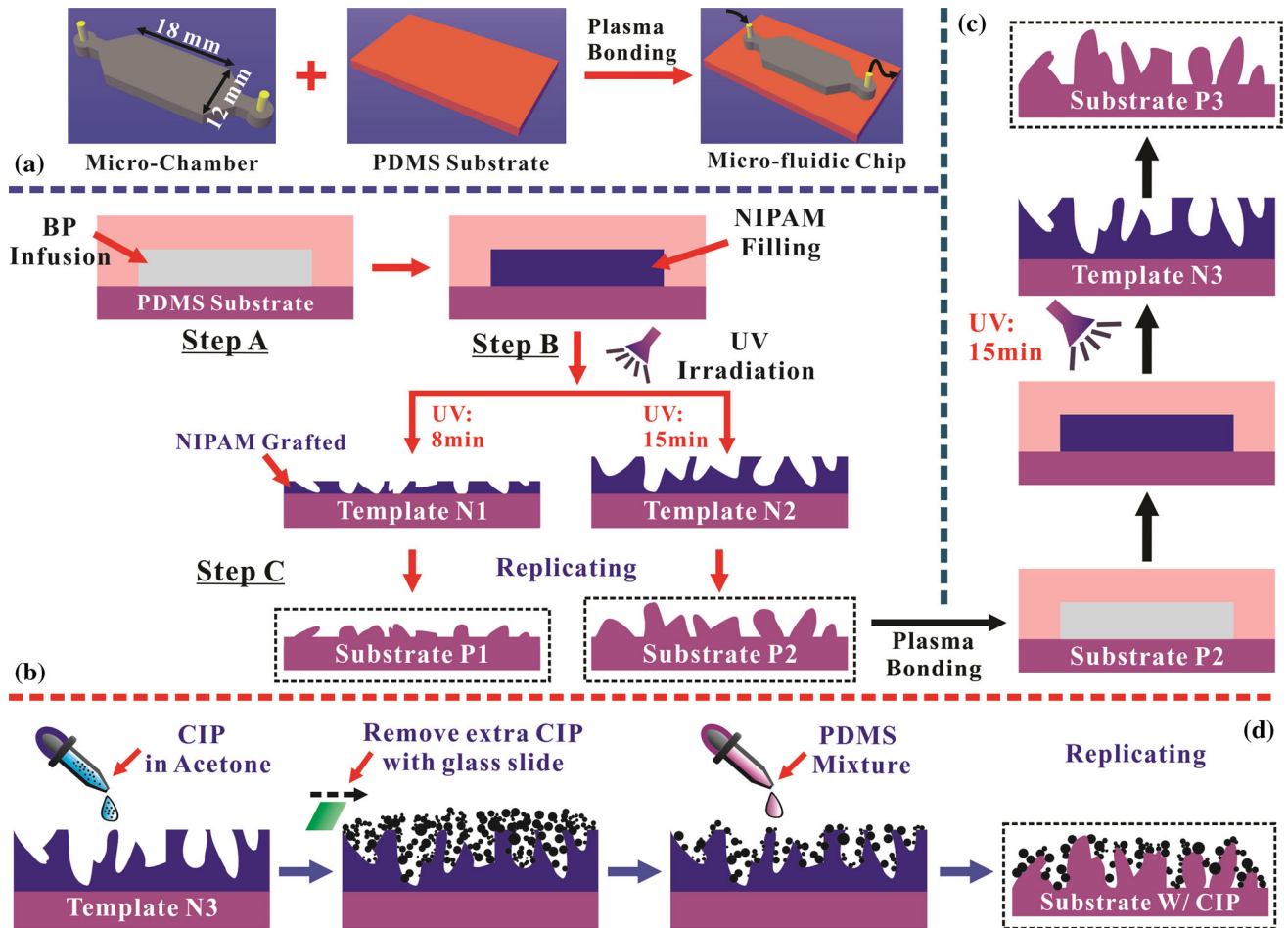


**Figure 1** **a** Schematic of preparation of microfluidic chamber for NIPAM grafting; **b** procedure of grafting NIPAM onto PDMS template via combinations of the microfluidic platform, photopolymerization, and PDMS replicating processes. The surface morphologies of PDMS substrates can be tuned by adopting different ultraviolet irradiation durations. Here, *step A* indicates BP injection. *Step B* means NIPAM filling and UV polymerization.

*Step C* is the PDMS casting process to transfer the surface morphology from the template to the PDMS substrate; **c** schematic of repeated grafting approach to further engineer the surface topologies of PDMS substrates based on template N2; and **d** process flow of incorporating carbonyl iron particles (CIP) onto the surface of PDMS sample for hierarchical architecture formation.

morphology. The PDMS substrates were thus named as P1 and P2 (indicated in Fig. 1b), indicating the UV duration of 8 and 15 min, respectively.

In order to further modify the surface topologies, a repeated grafting process was employed as provided in Fig. 1c. The reason to adopt the repeated grafting method instead of merely further increasing the UV illumination period is to avoid over-polymerization due to the overlaid exposure. As shown in Fig. 1c, a microfluidic chamber was bonded to substrate P2 for further repeated BP and NIPAM injection. After NIPAM grafting again (UV duration of 15 min) onto substrate P2, the obtained template was named as N3

and the PDMS substrate with duplicated surface morphology was denoted as P3.

### Preparation of PDMS substrates incorporated with CIP on surface

To form hierarchical architecture and regulate the surface adhesion property of PDMS substrates, we incorporated CIP into the preparation process as illustrated in Fig. 1d. Briefly, once the template, e.g., N3, was completed, drops of CIP suspensions (20 wt% in acetone) were continuously dipped to fully cover the NIPAM-grafted region on the template. The suspension was

agitated by a shaker (Vortex Genius 3, IKA) to promote the dispersion of CIP in acetone before each use. The drops will spread and fully cover the NIPAM-grafted template. After complete evaporation of acetone, the extra CIP was manually removed by a flat microscope slide (Sail Brand, China). As a result, residual CIP will adhere to the surface of the rough template as depicted in Fig. 1d. PDMS mixture was then slowly dripped onto the template, followed with degassing to completely remove the trapped air between the template and the PDMS mixture. After complete solidification, the PDMS sample was peeled off from the template, with amounts of CIP successfully embedded onto the upper surface. The NIPMA-grafted PDMS template was then flushed with acetone and scrapped with Kimwipes paper to remove the residual CIP for reuse. For all NIPAM-grafted PDMS templates (N1, N2, and N3), we can thus obtain two kinds of PDMS substrates correspondingly, with (W/) CIP or without (W/O) CIP.

### Characterizations

Contact angles (CA) of water droplet ( $\sim 5 \mu\text{L}$ ) on different PDMS substrates were measured via a digital microscope (VHX-1000, Keyence, Japan) at room temperature. Sliding angles (SA) are defined as the tilting angle at which the water droplet begins to roll off from the gradually inclined surface with the same experimental setup. Values of the CA and SA were analyzed via VHX-1000 commercial software and finalized as the average of measurements obtained from at least five samplings. High-resolution captures of surface morphologies of PDMS substrates were obtained via scanning electron microscopy (SEM, Sigma FE-SEM, Zeiss Corporation, Germany), where all the PDMS samples were sputtered with 30-nm platinum prior to observation. Atomic force microscopy (AFM, Dimension FastScan, Bruker Corporation, Massachusetts, USA) was used to analyze the surface topologies and roughness of the as-prepared PDMS substrates. The values of average roughness ( $R_a$ ) were obtained from at least three different locations with measured area of  $50 \times 50 \mu\text{m}^2$  in the tapping mode.

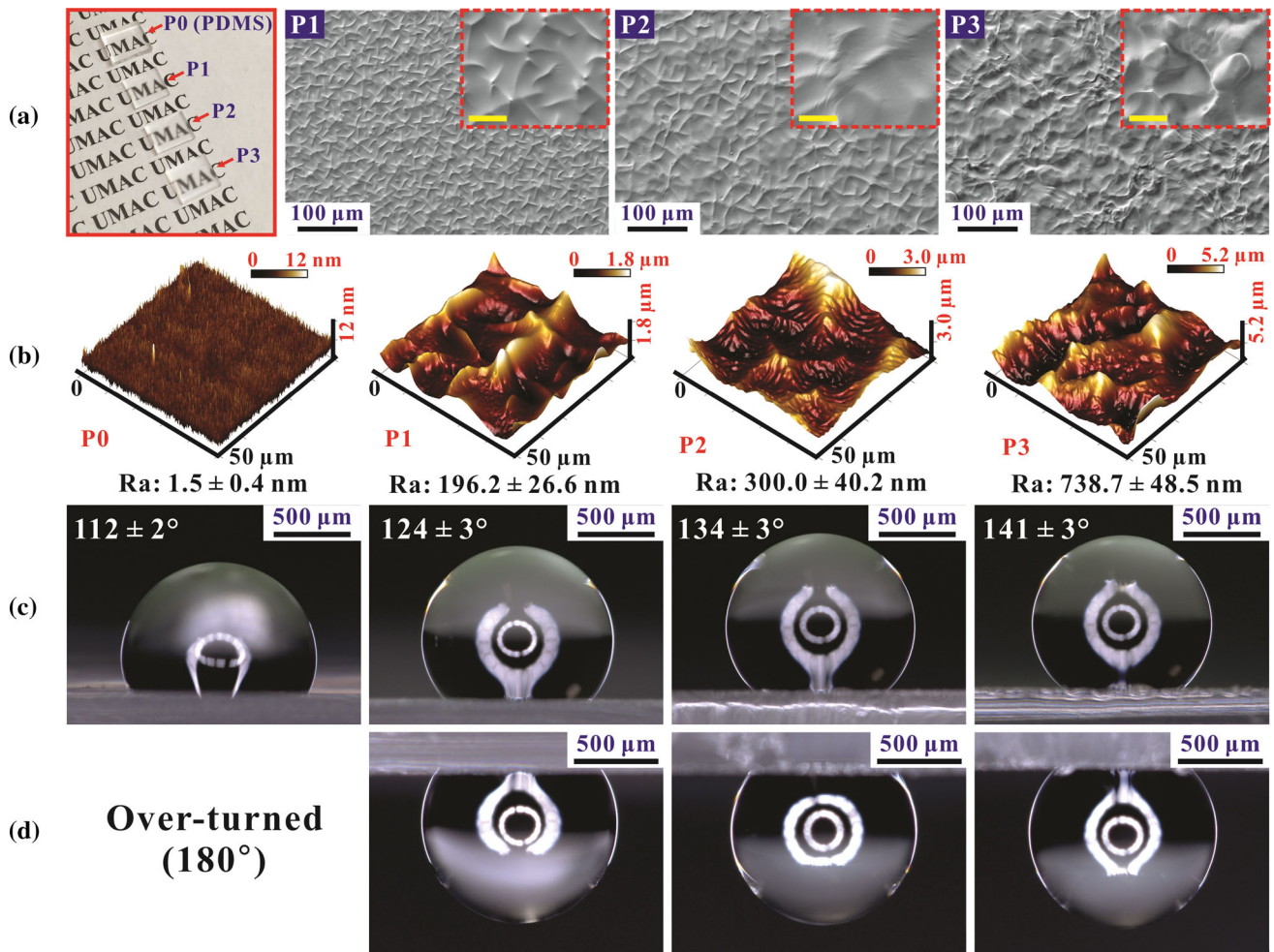
### Results and discussion

Figure 2a presents the real images of PDMS substrate P0, P1, P2, and P3. The substrates included here were all W/O incorporation of CIP on the surface. P0 is

native PDMS without surface roughness engineering. The transparency of the four samples was gradually decreased from P0 to P3, which might be originated from the increased degrees of surface roughness. The SEM images which clearly exhibit the surface morphologies of P1–P3 are provided in Fig. 2b, with insets to clearly exhibit the morphological difference among the as-prepared substrates. The surface morphologies were found to be more scabrous of substrate P3 when compared with the other two substrates. Further surface topological information was characterized via AFM as shown in Fig. 2b. For native PDMS substrate (P0), the average surface roughness ( $R_a$ ) was  $1.5 \pm 0.4 \text{ nm}$  which indicates as a highly smooth PDMS surface. For substrates P1 and P2, which are replicated from templates grafted with 8 and 15 min, the values of  $R_a$  were increased to  $196.2 \pm 26.6$  and  $300.0 \pm 40.2 \text{ nm}$ , respectively. For substrate P3 which was casted from NIPAM template with repeated grafting process, the value of  $R_a$  was dramatically increased to  $738.7 \pm 48.5 \text{ nm}$ .

The surface wetting characteristics of the as-prepared PDMS substrates W/O CIP are shown in Fig. 2c. When a  $\sim 5 \mu\text{L}$  micro-droplet was placed onto the native PDMS surface (P0), the recorded value of CA was  $112^\circ \pm 2^\circ$ . It was obviously recorded that the values of CA gradually increased to  $124^\circ \pm 3^\circ$  for substrate P1 and further reached  $134^\circ \pm 3^\circ$  for substrate P2, where the two substrates were replicated from NIPAM template with UV grafting duration of 8 and 15 min, respectively. Furthermore, via adopting a repeated grafting process, the observed value of CA on substrate P3 was dramatically increased to  $141^\circ \pm 3^\circ$ . The increment of CA might originate from the control of surface topologies which could facilitate a higher hydrophobicity with highly rough and extruded morphologies. Even increased surface hydrophobicity was found on the substrates W/O CIP, and we also noticed that all substrates mentioned above exhibited highly adhesive performance to the resident water droplets. As shown in Fig. 2d, the water droplets can still adhere to the surface even when the PDMS substrates were completely overturned.

We further investigated the surface wetting properties of substrates P1–P3 incorporated W/CIP. From Fig. 3a, we can observe the transmittance of as-prepared substrates has dramatically decreased from P1 to P3 due to the incorporation of CIP. The typical SEM images of three substrates were shown



**Figure 2** **a** Optical and SEM images of PDMS substrates P0, P1, P2, and P3, inserted with enlarged SEM images of higher magnifications (all scale bars for insets indicate 20  $\mu\text{m}$ ); **b** AFM images which present the surface roughness of substrates P0–P3, with corresponding  $R_a$  values as indicated; **c** static water contact

angles on PDMS substrates P0–P3 with corresponding real images of the resident droplets; and **d** the optical images of adhesive droplets on substrates P1–P3 when the substrates were completely overturned.

consequently, where we can clearly find the CIP incorporated to the substrate surface. In addition, the SEM images also indicate that the incorporated amount of CIP on the PDMS surface gradually increases from P1 to P3 (insets in Fig. 3a), which might be due to more trapped CIP on the template surface thanks to the increased extents of specific surface area. The AFM images in Fig. 3b clearly provide the surface topologies of substrates P1/P2/P3 when included with CIP on the surface. Compared with the substrates W/O CIP, all surface roughness degrees exhibited an obvious increase due to the inclusion of CIP and the surface hierarchical structures. Furthermore, we can clearly observe the amount of included CIP on substrate P3 is larger than

those on substrates P1 and P2. The values of CA on each substrate significantly increased when compared with the counterpart W/O CIP, as shown in Fig. 3c. For P1, CA has increased to  $137^\circ \pm 2^\circ$ , which can be considered to arise from the involvement of CIP on the upper surface of the substrate with more air traps. While for P2, CA has reached  $151^\circ \pm 3^\circ$ , which can be deemed as a superhydrophobic surface as defined in previous report [2]. The CA value of P3 incorporated with CIP was recorded to be  $160^\circ \pm 2^\circ$ , with almost  $20^\circ$  increment when compared to the counterpart W/O CIP. However, we found that the surface adhesion properties of P1–P3 revealed totally different phenomenon. For example, the water droplet can be still pinned on the surfaces of P1 and P2

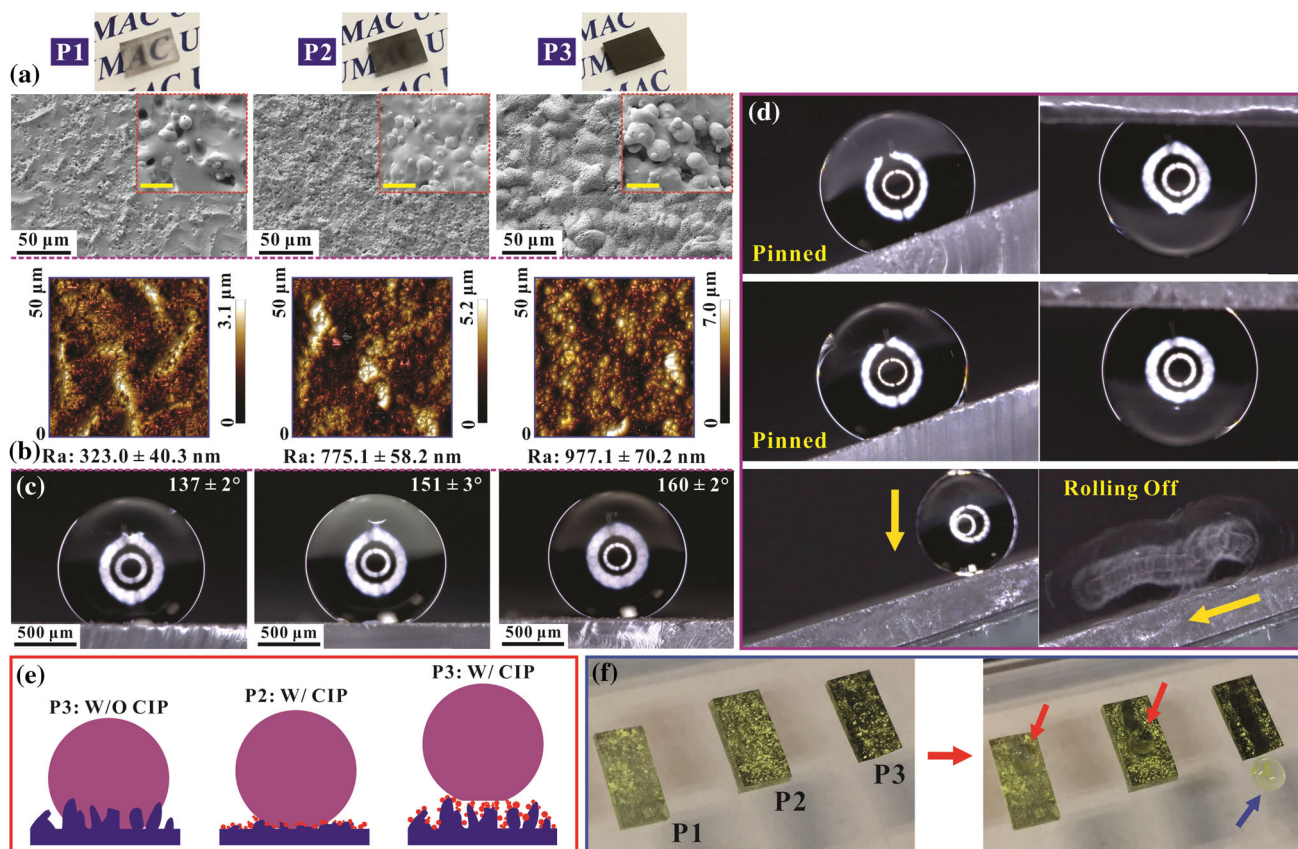


**Figure 3** **a** Optical and SEM images of PDMS substrates P1, P2, and P3 W/CIP, inserted with enlarged images of higher magnifications (*scale bars* of insets indicate 5  $\mu\text{m}$ ); **b** AFM images which present the surface roughness of substrates P0–P3 W/CIP, with corresponding  $R_a$  values as indicated; **c** static water contact angles on PDMS substrates P1–P3 W/CIP with corresponding real

images of the resident droplets; **d** optical images of water droplets on inclined/overturned substrates P1/P2 and rolling off water droplet on inclined substrate P3; **e** schematic of the different wetting and adhesion properties of the as-prepared PDMS substrates; and **f** comparison of the self-cleaning performance of the three substrates incorporated with CIP.

even when the substrates were inclined with  $\sim 20^\circ$  or totally overturned as provided in Fig. 3d. While for substrate P3, the water droplet can easily roll off from the surface inclined with  $20^\circ$  once loaded to the substrate. The results confirmed that even W/CIP, substrates P1 and P2 still exhibit highly adhesive capability to the resident water droplets while substrate P3 reversely displayed low adhesion to the resident drop.

A possible schematic for this phenomenon is illustrated in Fig. 3e. The obvious adhesion difference on the as-prepared surfaces can be mainly attributed to the distinct states of the water droplet on the PDMS substrate. For substrate P3 W/O CIP, the resident water droplet can easily penetrate into the voids of the surface protuberance, leading to a highly adhesive force and relatively low contact angle ( $\sim 141^\circ$ ). Such status is well known as the ‘Wenzel

state,’ where the droplet can wet the contact area and pin into the rough surface, resulting in a high water adhesion property as observed in the experiment. While for substrate P3 W/CIP, the dramatically increased surface topology accompanied with CIP can result in the ‘Lotus effect’ which exhibits superhydrophobic ( $\text{CA} > 150^\circ$ ) and low surface adhesion. For this case, the resident droplet will only contact with the peaks of the hierarchical morphologies on the surface, with air layer effectively trapped between the solid surface and the water droplet. The superhydrophobic status with low adhesion is also known as ‘Cassie State’ where the resident droplet can easily roll off from the surface with a small inclined angle as shown in Fig. 3d. As the surface topology of P2 was not sufficient to support the resident droplet, the drop will still penetrate to the surface even when the surface has been incorporated

with W/CIP. Consequently, we can observe the superhydrophobic property of substrate P2 W/CIP with high adhesion, which is well known as the ‘Petal effect.’ Thanks to the low adhesion of P3 W/CIP, we further experimentally confirmed the self-cleaning function as shown in Fig. 3f. For substrates P1, P2, and P3 W/CIP, the surface has been purposely covered with dust (yellow nanoparticles) and placed on an inclined glass slide. When a water droplet ( $\sim 10 \mu\text{L}$ ) was released from the pipette to the surface of the substrate, the droplet can swiftly roll off from the substrate P3, with completely removing the dust through the moving path (as indicated by the blue arrow). However, the water droplets were sticky on the surface of P1 and P2 without rolling off (as indicated by the red arrows).

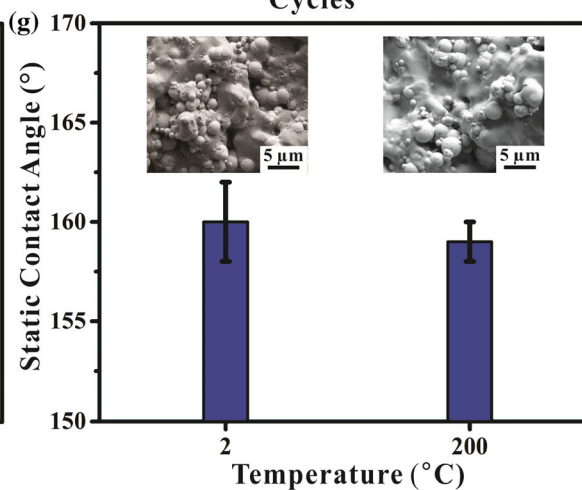
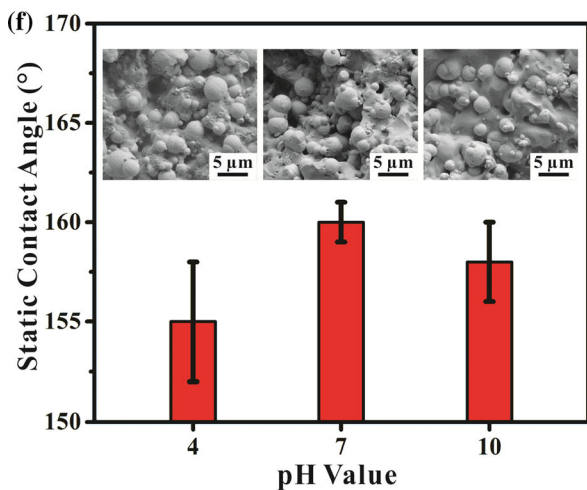
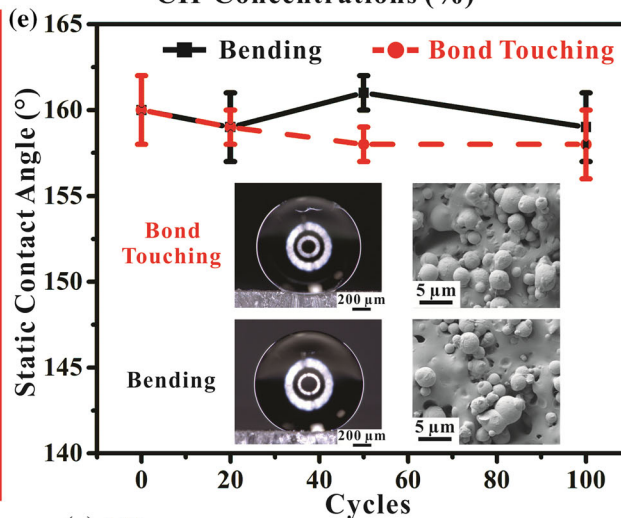
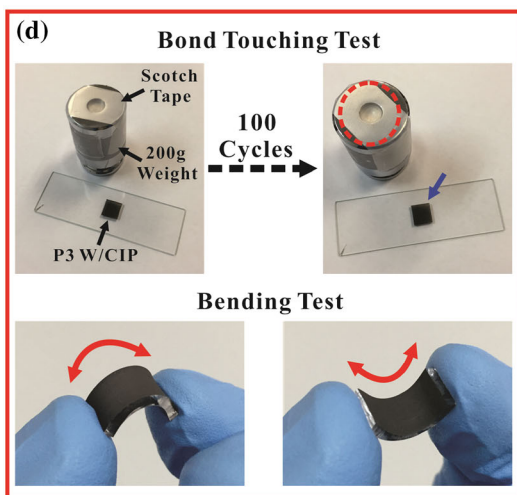
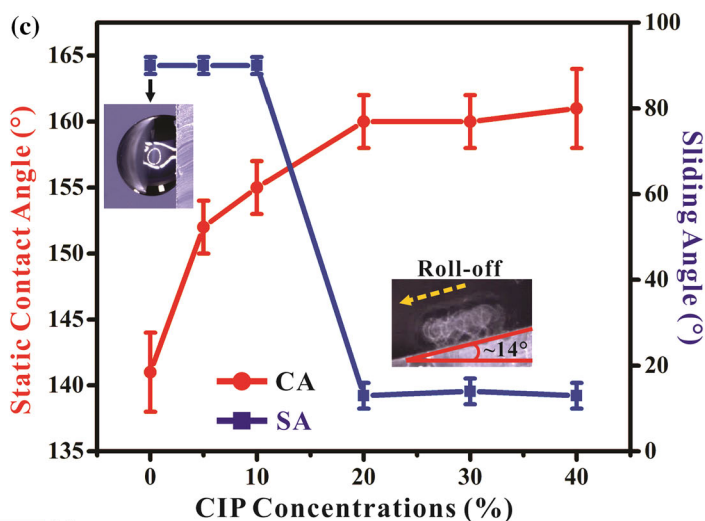
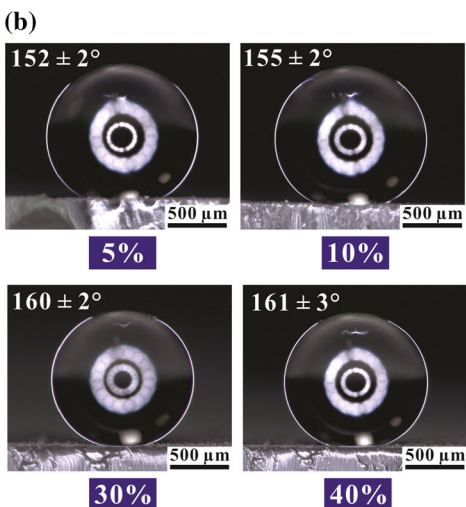
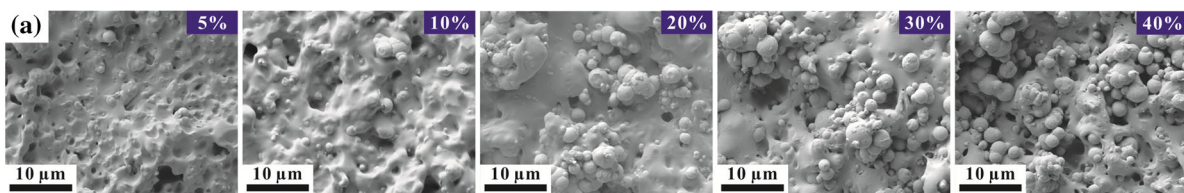
The effect of applied CIP concentrations on the surface adhesion and wetting characteristics was further systematically investigated. Figure 4a presents the SEM images of substrate P3 W/CIP of different suspension concentrations ranging from 0 to 40 wt%. It can be found that for the suspension concentrations of 5 and 10 wt%, only a few particles can be observed on the substrate surface from the SEM image. The amounts of incorporated CIP gradually increased as the concentration increased from 5 to 40 wt%. The static contact angles on the substrates are presented in Fig. 4b and c. For relatively lower suspension concentrations (0–10 wt%), the values of CA gradually increased from  $141^\circ$  to  $155^\circ$  (0 wt% means P3 W/O CIP). While for concentrations of 20–40 wt%, we cannot obviously figure out the tendency of CA and the values keep almost as constant around  $160^\circ$ . Additionally, the sliding angles exhibit extreme differences between lower (typically smaller than 10 wt%) and higher CIP concentrations. From the blue curve, we can observe that even when the substrates were placed vertically, the water droplets can still adhere on the surface for concentrations smaller than 20 wt% (as inserted image shown). However, the water droplets can easily roll off from the substrates when the substrates were gradually inclined to angles of  $\sim 14^\circ \pm 2^\circ$  for suspension concentrations of 20, 30, and 40 wt% as shown in the inserted images. We can conclude that the included CIP amount plays an important role in the distinct adhesion difference, where the low suspension concentrations are incapable to provide sufficient supports to form the air layer and thus the resident droplet will tend to impregnate into the surface area.

**Figure 4** a SEM images of substrate P3 incorporated W/CIP from different concentrations of CIP suspensions; b optical images of water droplets on substrates P3 W/different concentrations of CIP; c dependence curves between the CIP concentrations and the contact angle (red plot) and sliding angle (blue plot) are also provided; d schematic illustration of the mechanical stability evaluation of the substrate P3 W/CIP via bond touching and bending tests; e dependence of static water contact angles of substrate P3 W/CIP on the bond touching cycles and bending cycles. The insets provide the resident water droplet images and SEM images after 100 cycles’ bond touching test and bending test, respectively; f contact angles of P3 W/CIP after immersion into solutions with different pH values for 24 h; and g contact angles of P3 W/CIP exposed to different temperatures for 12 h.

However, the amount of included CIP can increase correspondingly with further higher suspension concentrations to effectively produce the hierarchical structure for the Cassie state. The results experimentally strengthened the influences of the CIP existences on the surface adhesion capabilities of PDMS substrates, which indicates the synergetic effect of the surface roughness and CIP involvement is critical in the surface adhesion and wetting property.

Mechanical stability is one important criterion to evaluate the potential of the as-prepared superhydrophobic substrates for practical applications [40, 41]. To verify the CIP adhesion within PDMS matrix, we used scotch tape to test the bond properties of the PDMS surface as shown in Fig. 4d. A piece of scotch tape was tightly attached to the bottom of a weight (200 g) and vertically bonded to touch the sample surface under  $\sim 20 \text{ kPa}$  (the surface area of the test sample is  $\sim 1 \text{ cm}^2$  here). The weight along with the scotch tape was then taken away to perform various repeated bond touching cycles for stability evaluation. After 100 cycles’ test, no obvious CIP detachment from the substrate was observed as indicated by the dashed round circle (in red) and the arrow (in blue). A further bending test was carried out to assess the stability of the substrate under mechanical deformations. Different bending/stretching cycles were also performed to testify the wetting characteristics and structural variation of the substrate P3 W/CIP. As shown in Fig. 4e, the values of WCA remained almost the same after 20, 50, and 100 cycles’ bending testing and only a slight decrease ( $\sim 2^\circ$ ) of WCA was disclosed after periodic bond touching tests. The SEM images also confirmed the fact of no obvious surface





structural deformation and a large amount of CIPs were still incorporated within the PDMS matrix. The excellent mechanical stability of the as-prepared samples might originate from the presented method, where the procedure of CIP incorporation into the PDMS matrix was prior to the step of thermal solidification. Consequently, the particles could firmly integrate to the upper surface of PDMS substrate during the thermal solidification process instead of physically adhering to the solid PDMS surface. In addition to the mechanical resistance, we further investigated the chemical and thermal stability to test the durability of the substrates under different circumstances [42, 43]. The substrates (P3 W/CIP) were simultaneously immersed into solutions with different pH values (potassium hydrogen phthalate, mixed phosphate, and sodium tetraborate with pH of 4, 7, and 10) under room temperature for 24 h and then washed with deionized water for further surface characterization. The SEM insets in Fig. 4f exhibit no obvious changes of the surface hierarchical structures for all samples. No drastic change in the water contact angles was found for substrates under neutral and alkaline conditions. A small contact angle decrease ( $\sim 4^\circ$ ) could be observed for the substrate under acidic condition, which might be attributed to the slight corrosion/oxidation of the substrate surface within the acidic environment. Figure 4g provides the SEM images and contact angle changes of the substrates under different temperatures, 2 °C (in refrigerator) and 200 °C (on hotplate) for 12 h, respectively. No drastic contact angle changes were found for both conditions, and we could also confirm from the SEM images that the particles could still be included in the PDMS matrix to retain the hierarchical structures. From this perspective, the particles could still be firmly included within the rough PDMS substrate matrix exhibiting durable chemical and thermal stabilities under different harsh environmental conditions.

As indicated in Figs. 2d and 3e, the adhesive characteristics of PDMS substrates can be flexibly regulated from two approaches. For example, the substrate P3 W/O CIP can exhibit highly adhesive capability to resident water droplet and transform to low adhesion to water droplet when incorporated with CIP. The adherent performances of substrate P3 W/ W/O CIP are further confirmed as shown in Fig. 5a. From the optical image, we can clearly observe the rebounding water stream when hitting on

the surface of P3 W/CIP (the bottom image). While for P3 W/O CIP, the rebounding phenomenon cannot be observed and water fell along the substrate surface. Consequently, by selectively incorporating CIP to the PDMS surface within desired regions, we can swiftly regulate the substrate with different adhesion distributions and thus control the distance of the droplet transportation path. By regionally covering the NIPAM-grafted template, we can dip CIP suspensions onto the uncovered area for acetone evaporation and CIP sedimentation. Followed with PDMS pouring and baking process, the PDMS samples can be peeled off from the template with regional CIP incorporation. Figure 5b presents four substrates (P3) with distinctly regional CIP incorporation, where the black part on the right of each sample indicates the CIP has been combined. From the image, we can clearly find the interface between the high adhesion (left part) and the low adhesion (right part) based on the existence of CIP. With the design of the partially low adhesive surface, water droplet could thus easily slide from the low adhesion part and stop motion when reaching the high adhesive region, as illustrated in Fig. 5c. The top images in Fig. 5d show that the water droplets can roll off from the top of the substrates to the highly adhesive region, which means that this platform can be used for quantitative transporting distance of water droplets for real applications. The video recording the controlled water sliding phenomenon can be found in the supplementary electronic information (SVideo-1). However, due to the high adhesion force of the parts W/O CIP, the water droplets quickly stuck to the PDMS surface when loaded onto the surfaces as presented in the bottom images of Fig. 5d. It should be noted here that the variable adhesion design can be simply achieved by partially covering the template surface during the CIP loading process, indicating that the presented approach can be conveniently adopted for fields where the motion control of water droplet is of great importance.

Inspired by the water adhesion difference between substrates P2 W/CIP and P3 W/CIP, another method to achieve patterned adhesive difference is by generating patterned roughness divergence and then applying CIP for hierarchical adhesion formation. As illustrated in Fig. 5e, after obtaining the substrate P2 (W/O CIP), the substrate was bonded to another PDMS micro-chamber to form sealed

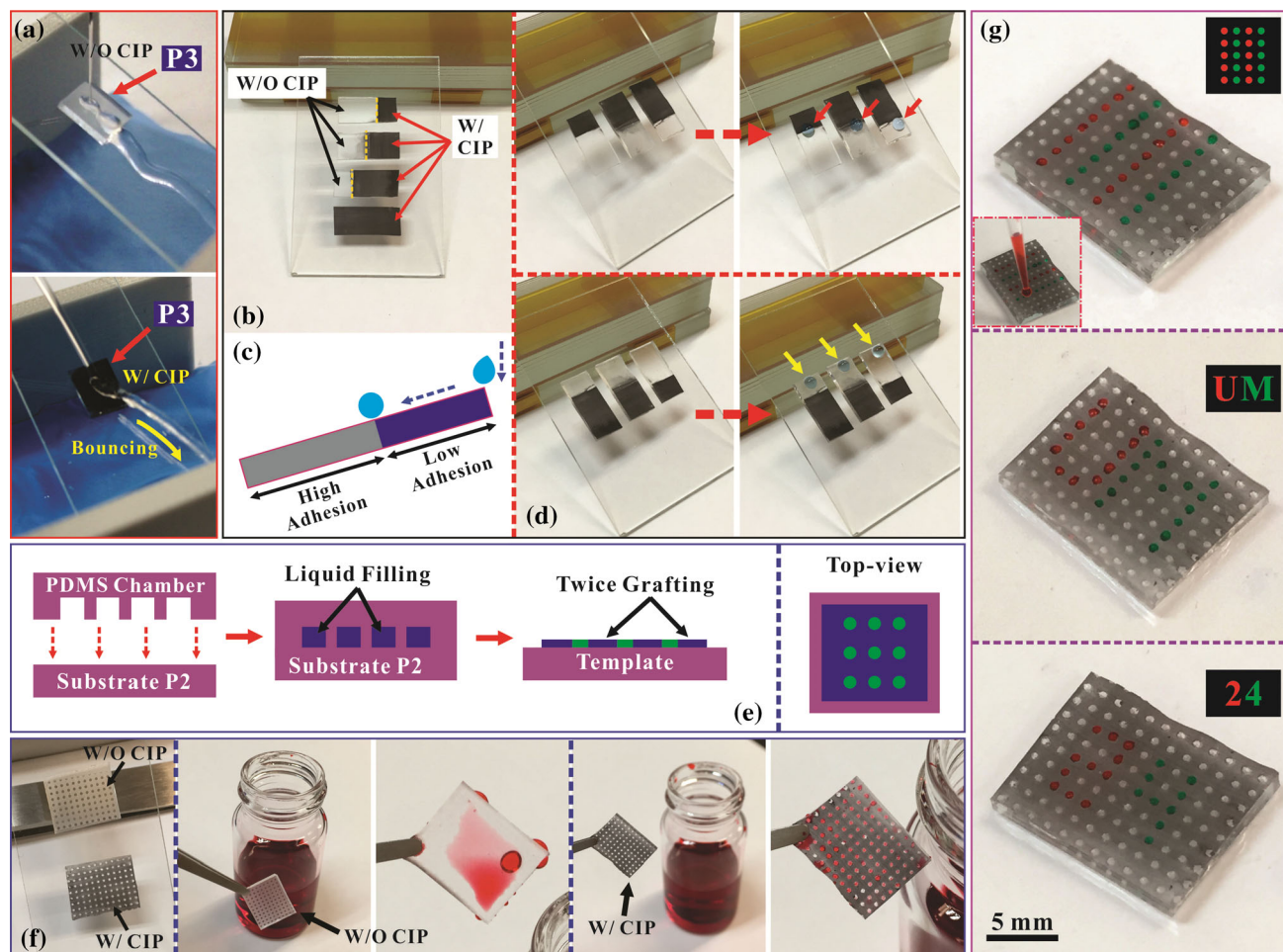


**Figure 5** **a** Adhesive property of substrate P3 W/and W/O CIP. The substrate P3 W/CIP exhibits rebounding water streams; **b** optical images of selectively incorporated CIP on substrate P3; **c** schematic of controlled rolling distance by combination of low and high adhesive surface on a single inclined substrate; **d** the controlled rolling droplets on P3 substrates with selectively

incorporated CIP; **e** brief schematic of preparation of NIPAM template with patterned grafting; **f** optical images of substrate with patterned adhesive properties for rapid droplet formation; and **g** digital droplet localization based on the PDMS substrate incorporated with CIP and patterned surface water adhesion.

microfluidic device for BP and NIPAM injection. Unlike the micro-chamber that we used in Fig. 1, here the micro-chamber has been designed with micro-pillar arrays inside, which means that after plasma bonding, the PDMS micro-pillar arrays will be also bonded to the substrate P2. The preparation process of such kind of micro-chamber is identical with the one in Fig. 1a via standard soft lithography. In this work, the diameter of the micro-pillars was set as 500  $\mu\text{m}$  and the center-to-center pitch was defined to 1 mm. Detailed design layout of the micro-chamber integrated with micro-pillar arrays can also be referred to the supplementary information. Consequently, with repeated steps A–C illustrated in Fig. 1, we can successfully selectively graft NIPAM to the regions

within the micro-chamber that are uncovered by the micro-pillar arrays. As indicated in Fig. 5e, the resultant blue regions on the template mean that such regions have been grafted with NIPAM twice, while the green districts stand for the regions only grafted one time (the same as substrate P2). Followed with CIP incorporation process, we can simply obtain substrates with patterned adhesion variations as shown in Fig. 5f. The left panel provided the optical images of the obtained substrates W/O and W/CIP. To prove the novel adhesive performance, we carefully immersed the substrates into the bottle containing of red dyed aqueous solution. It can be clearly found that for the substrate W/O CIP, almost all the surface of the substrate was covered with water after

taken out from the bottle. This means that a patterned adhesion property is still hard to achieve without incorporation of CIP onto the substrate. However, for the substrate W/CIP, water only adheres on the regions that were only grafted with NIPAM for one time after taking the substrate out from the bottle. For the regions that have been grafted twice, it is clear that no liquids are attached and thus droplet arrays can be easily achieved by simply dipping the substrate into the solution. The current results are also in well consistency with the statement from Fig. 3, where the circular arrays are equal to the roughness degrees of substrate P2 W/CIP and the regions outside the circles stands for P3 W/CIP, thus leading to patterned adhesion divergence of the resultant substrate. Thanks to the patterned adhesion matrix, we can simply pattern water droplets on the substrate via manually using pipette for liquid loading as shown in Fig. 5g. When a pipette filled with reagents moves across the surface of the substrate, only the circles with high water adhesion will attract small volumes of liquids (microliter scales) from the tip of the pipette. On the other hand, the pipette along with the solution will pass by the regions with low adhesive properties without leaving liquids. Additionally, via adopting different kinds of reagents, we can swiftly load different reagents to desired locations. The top figure shows the lines with two different reagents can be achieved (the liquids containing red and green dyes are used here for better observation). Such platform can also be applied to flexibly pattern analytes/reactants with desirable characters, e.g., UM (central figure), 24 (bottom figure). The video recording the facile droplet localization via manual loading can be found in the supplementary electronic information (SVideo-2). We believe that via combination with digital reagent loading controller, the presented substrates can act as a powerful platform for rapid and precise droplet formation and further bio/chemical diagnosis.

## Conclusions

In summary, we have successfully developed a versatile and economic approach to prepare superhydrophobic PDMS substrates with controllable water adhesion capability without any elaborate nano-fabrication and surface post-modification processes. Initially via surface grafting of NIPAM onto PDMS as

a template, the replicated PDMS substrates can only obtain increased CA values due to the modified surface roughness degrees while lack of control on the water adhesion. Via applying CIP suspensions onto the template, the surface morphology can be fully transferred to the PDMS specimen incorporated with CIP. On account of the synergistic effect from the surface roughness and CIP incorporation, the water adhesion capabilities of the PDMS substrates can be flexibly tuned ranging from droplet pinning (Wenzel state) to excellent water repellency (Cassie state). The basic mechanism was evaluated to describe the water adhesion difference among different PDMS substrates, where the low water adhesion might arise from the hierarchical micro- and quasi-nano-structures on the rough PDMS substrates due to the presence of CIP. The strategy was further exploited to create substrates with regional water adhesion divergence to control droplet transportation. Patterned water adhesion was successfully achieved and applied for convenient droplet formation or programmable water droplet localization on specific positions. On the basis of the unique advantages as mentioned above, we believe that the described avenue for preparation of superhydrophobic PDMS substrates with controllable water adhesion can be of great potential in future practical applications such as droplet controlling, lab-on-chip device, and biological trace analysis.

## Acknowledgements

The authors appreciate the support of the Science and Technology Development Fund from Macau SAR (FDCT-073/2016/A2) and Start-up Research Grant (SRG2016-00067-FST) from the Research & Development Administration Office at University of Macau.

**Electronic supplementary material:** The online version of this article (doi:[10.1007/s10853-017-1317-x](https://doi.org/10.1007/s10853-017-1317-x)) contains supplementary material, which is available to authorized users.

## References

- [1] Lafuma A, Quéré D (2003) Superhydrophobic states. *Nat Mater* 2:457–460

- [2] Wang ST, Jiang L (2007) Definition of superhydrophobic states. *Adv Mater* 19:3423–3424
- [3] Darmanin T, Guittard F (2015) Superhydrophobic and superoleophobic properties in nature. *Mater Today* 18:273–285
- [4] Li SH, Huang JY, Chen Z, Chen GQ, Lai YK (2017) A review on special wettability textiles: theoretical models, fabrication technologies and multifunctional applications. *J Mater Chem A* 5:31–55
- [5] Feng L, Li SH, Li YS, Li HJ, Zhang LJ, Zhai J, Song YL, Liu BQ, Jiang L, Zhu DB (2002) Super-hydrophobic surfaces: from natural to artificial. *Adv Mater* 14:1857–1860
- [6] Simpson JT, Hunter SR, Aytug T (2015) Superhydrophobic materials and coatings: a review. *Rep Prog Phys* 78:086501
- [7] Song C, Zheng YM (2014) Wetting-controlled strategies: from theories to bio-inspiration. *J Colloid Interface Sci* 427:2–14
- [8] Yang HL, Liang FX, Chen Y, Wang Q, Qu XZ, Yang ZZ (2015) Lotus leaf inspired robust superhydrophobic coating from strawberry-like Janus particles. *NPG Asia Mater* 7:e176
- [9] Bai X, Xue CH, Jia ST (2016) Surfaces with sustainable superhydrophobicity upon mechanical abrasion. *ACS Appl Mater Interfaces* 8:28171–28179
- [10] Park HK, Yoon SW, Do YR (2012) Superhydrophobicity of 2D SiO<sub>2</sub> hierarchical micro/nanorod structures fabricated using a two-step micro/nanosphere lithography. *J Mater Chem* 22:14035–14041
- [11] Li XM, Reinhoudt D, Crego-Calama M (2007) What do we need for a superhydrophobic surface? A review on the recent progress in the preparation of superhydrophobic surfaces. *Chem Soc Rev* 36:1350–1368
- [12] Fürstner R, Barthlott W, Neinhuis C, Walzel P (2005) Wetting and self-cleaning properties of artificial superhydrophobic surfaces. *Langmuir* 21:956–961
- [13] Guo ZG, Liu WM, Su BL (2011) Superhydrophobic surfaces: from natural to biomimetic to functional. *J Colloid Interface Sci* 353:335–355
- [14] Chen N, Pan QM (2013) Versatile fabrication of ultralight magnetic foams and application for oil–water separation. *ACS Nano* 7:6875–6883
- [15] Sasmal AK, Mondal C, Sinha AK, Gauri SS, Pal J, Aditya T, Ganguly M, Dey S, Pal T (2014) Fabrication of superhydrophobic copper surface on various substrates for roll-off, self-cleaning, and water/oil separation. *ACS Appl Mater Interfaces* 6:22034–22043
- [16] McHale G, Shirtcliffe NJ, Newton MI (2004) Contact-angle hysteresis on super-hydrophobic surfaces. *Langmuir* 20:10146–10149
- [17] Feng L, Zhang YN, Xi JM, Zhu Y, Wang N, Xia F, Jiang L (2008) Petal effect: a superhydrophobic state with high adhesive force. *Langmuir* 24:4114–4119
- [18] Liu XJ, Liang YM, Zhou F, Liu WM (2012) Extreme wettability and tunable adhesion: biomimicking beyond nature? *Soft Matter* 8:2070–2086
- [19] Jin MH, Feng XJ, Feng L, Sun TL, Zhai J, Li TJ, Jiang L (2005) Superhydrophobic aligned polystyrene nanotube films with high adhesive force. *Adv Mater* 17:1977–1981
- [20] Mertaniemi H, Jokinen V, Sainiemi L, Franssila S, Marmur A, Ikkala O, Ras RHA (2011) Superhydrophobic tracks for low-friction, guided transport of water droplets. *Adv Mater* 23:2911–2914
- [21] Zamuruyev KO, Bardaweel HK, Carron CJ, Kenyon NJ, Brand O, Delplanque JP, Davis CE (2014) Continuous droplet removal upon dropwise condensation of humid air on a hydrophobic micropatterned surface. *Langmuir* 30:10133–10142
- [22] Chen KL, Zhou SX, Wu LM (2016) Self-healing underwater superoleophobic and antibiofouling coatings based on the assembly of hierarchical microgel spheres. *ACS Nano* 10:1386–1394
- [23] Hong X, Gao XF, Jiang L (2007) Application of superhydrophobic surface with high adhesive force in no lost transport of superparamagnetic microdroplet. *J Am Chem Soc* 129:1478–1479
- [24] Park YM, Gang M, Seo YH, Kim BH (2011) Artificial petal surface based on hierarchical micro- and nanostructures. *Thin Solid Films* 520:362–367
- [25] Hu HB, Yu SX, Song D (2016) No-loss transportation of water droplets by patterning a desired hydrophobic path on a superhydrophobic surface. *Langmuir* 32:7339–7345
- [26] Balu B, Berry AD, Hess DW, Breedveld V (2009) Patterning of superhydrophobic paper to control the mobility of microliter drops for two-dimensional lab-on-paper applications. *Lab Chip* 9:3066–3075
- [27] Yong JL, Yang Q, Chen F, Zhang DS, Farooq U, Du GQ, Hou X (2014) A simple way to achieve superhydrophobicity, controllable water adhesion, anisotropic sliding, and anisotropic wetting based on femtosecond-laser-induced line-patterned surfaces. *J Mater Chem A* 2:5499–5507
- [28] Elsharkawy M, Schutzius TM, Megaridis CM (2014) Inkjet patterned superhydrophobic paper for open-air surface microfluidic devices. *Lab Chip* 4:1168–1175
- [29] Xia YN, Whitesides GM (1998) Soft lithography. *Annu Rev Mater Sci* 28:153–184
- [30] Berthier E, Young EWK, Beebe D (2012) Engineers are from PDMS-land, Biologists are from polystyrenia. *Lab Chip* 12:1224–1237

- [31] Cao CY, Ge MZ, Huang JY, Li SH, Deng S, Zhang SN, Chen Z, Zhang KQ, Al-Deyab SS, Lai YK (2016) Robust fluorine-free superhydrophobic PDMS-orosil@fabrics for highly effective self-cleaning and efficient oil–water separation. *J Mater Chem A* 4:12179–12187
- [32] Wang Q, Yu MG, Chen GX, Chen QF, Tian JF (2017) Robust fabrication of fluorine-free superhydrophobic steel mesh for efficient oil/water separation. *J Mater Sci* 52:2549–2559. doi:10.1007/s10853-016-0548-6
- [33] Yong JL, Chen F, Yang Q, Zhang DS, Bian H, Du GQ, Si JH, Meng XW, Hou X (2013) Controllable adhesive superhydrophobic surfaces based on PDMS microwell arrays. *Langmuir* 29:3274–3279
- [34] Zhang ES, Wang YS, Lv T, Li L, Cheng ZJ, Liu YY (2015) Bio-inspired design of hierarchical PDMS microstructures with tunable adhesive superhydrophobicity. *Nanoscale* 7:6151–6158
- [35] Huang XJ, Kim DH, Im M, Lee JH, Yoon JB, Choi YK (2009) ‘Lock-and-key’ geometry effect of patterned surfaces: wettability and switching of adhesive force. *Small* 5:90–94
- [36] Wu D, Wu SZ, Chen QD, Zhang YL, Yao J, Yao X, Niu LG, Wang JN, Jiang L, Sun HB (2011) Curvature-driven reversible in situ switching between pinned and roll-down superhydrophobic states for water droplet transportation. *Adv Mater* 23:545–549
- [37] Roy PK, Pant R, Nagarajan AK, Khare K (2016) Mechanically tunable slippery behavior on soft poly(dimethylsiloxane)-based anisotropic wrinkles infused with lubricating fluid. *Langmuir* 32:5738–5743
- [38] Jin MH, Feng XJ, Xi JM, Zhai J, Cho K, Feng L, Jiang L (2005) Super-hydrophobic pdms surface with ultra-low adhesive force. *Macromol Rapid Commun* 26:1805–1809
- [39] Feng XJ, Jiang L (2006) Design and creation of superwetting/antiwetting surfaces. *Adv Mater* 18:3063–3078
- [40] Chen KL, Zhou SX, Yang S, Wu LM (2015) Fabrication of all-water-based self-repairing superhydrophobic coatings based on UV-responsive microcapsules. *Adv Funct Mater* 25:1035–1041
- [41] Li BC, Zhang JP (2016) Durable and self-healing superamphiphobic coatings repellent even to hot liquids. *Chem Commun* 52:2744–2747
- [42] Xue CH, Bai X, Jia ST (2016) Robust, self-healing superhydrophobic fabrics prepared by one-step coating of PDMS and octadecylamine. *Sci Rep* 6:27262
- [43] Zhang F, Shi ZW, Jiang YJ, Xu CY, Wu ZH, Wang YY, Peng CS (2017) Fabrication of transparent superhydrophobic glass with fibered-silica network. *Appl Surf Sci* 407:526–531